Acta Biomed 2024; Vol. 95, N. 1: e2024009 DOI: 10.23750/abm.v95i1.14104

Original article

Synthetic MRI of prostate: correlation of T1 and T2-mapping with PI-RADS v2 scores

Giuseppe Corrias[1], Giorgia Sanna[1], Laura Eusebi[2], Valentina Testini[3,4], Antonello De Lisa[5], Giuseppe Guglielmi[3,4,6], Luca Saba[1]

[1]Department of Radiology, University of Cagliari, Cagliari, Italy; [2]Radiology Unit, "Carlo Urbani" Hospital, Jesi, Italy; [3]Department of Clinical and Experimental Medicine, Foggia University School of Medicine, Foggia, Italy; [4]Radiology Unit, "Dimiccoli" Hospital, Barletta, Italy; [5]Department of Urology, University of Cagliari, Cagliari, Italy; [6]Radiology Unit, IRCCS "Casa Sollievo della Sofferenza" Hospital, San Giovanni Rotondo, Italy

Abstract. *Background and aim:* There has been a drive to develop methods of quantitative Magnetic Resonance Imaging (MRI) imaging such as the calculation of T1 and T2 relaxation times and ADC values from diffusion-weighted imaging (DWI) to develop imaging biomarkers that complement subjective radiological assessment. This retrospective study aims to evaluate if T1 and T2 relaxation times are significant predictors of malignancy, correlating them with the PI-RADS v2 scores. *Methods:* This is a retrospective, monocentric, observational study, which included 33 consecutive patients with clinically significant prostatic cancer subjected to prostate MRI by regular clinical practice. We used T1 MP2RAGE and T2-multi-TE FSE 2D sequences with a reconstruction of T1 and T2 maps at the dedicated workstation. Lesions were identified by a radiologist who attributed the PI-RADSv2 score and then traced the Regions-of-Interest (ROI)also in the corresponding areas of healthy tissue. Wilcoxon signed-rank test in fixed ranks was used for comparison. *Results:* We found statistically significant differences between relaxation time of the tumor and healthy tissue of the peripheral zone (PZ) (T1maps: p=0.043) (T2maps: p=0.043), and the transition zone (TZ) (T1maps: p=0.018) (T2maps: p=0.062). The Spearman test shows a tendency to a correlation between relative PI-RADS scores and T2-times within the peripheral zone(p=0.060) and T1-times within the transition zone (p-value=0.053). *Conclusions*: There is a significant difference between the T1 and T2-relaxation times of pathological tissue and that of healthy prostate, both for lesions in the TZ as well as in the PZ. This reflects the intrinsic physical characteristics of the analyzed tissues represented as relaxation times of transverse and longitudinal magnetization. There is also a tendency to a correlation between PIRADS scores and T1/T2 relaxation times. (www.actabiomedica.it)

Key words: quantitative MRI, synthetic MRI, functional magnetic resonance imaging, prostate cancer, T1 mapping, T2 mapping

Introduction

In recent years multiparametric Magnetic Resonance Imaging (mpMRI) has advanced to an progressively early part in the work-up of patients with suspicion of prostate tumor (1,2,3). The identification of tumor tissue within the prostate is reliant on the radiologist's ability to distinguish between tumor and normal prostatic tissue by evaluating T2w imaging, Diffusion-Weighted Imaging (DWI), and Dynamic Contrast-Enhanced (DCE) imaging. The creation of the Prostate Imaging–Reporting and Data System (PI-RADS) for prostate MRI (4) has contributed to more standardized exams, interpretation, and

reporting of prostate MRI. The PIRADS classification has been updated in 2015 and 2019 (with its latest version, PIRADS 2.1) and it is still growing, based on recent publications on mpMRI of the prostate (5,6).

For the peripheral zone (PZ), the DWI is the primary influential sequence (dominant technique) and it is associated with DCE images to assign the PI-RADS score.

The transition zone (TZ) is around the prostatic urethra, and in elderly benign prostatic hyperplasia (BPH) causes an enlargement of this zone. For the TZ, T2w imaging is the most influential sequence to be associated to DWI/ADC to assign the PI-RADS score. Identification of the location of a lesion is paramount because the main sequence for PI-RADS valuation in the PZ is different from the TZ.

The ADC value of a given lesion is inversely correlated to the probability of that lesion to be a malignant tumor. Values higher than 1000 mm2/s are probably benign and lower than 750 mm2/s, probably malignant. However, these values are not absolute and can change substantially between different vendors and scanners.

A lesion is considered to have restricted DWI only when high intensity on high b values is accompanied by a low intensity on the ADC maps, and in that case the lesion is considered to be highly cellulated and thus malignant (7,8).

However, the application of the PI-RADS assessment system in different clinical settings has been shown to be highly variable and not objective, regardless the presence of definite interpretation guidelines of MRI of the prostate (9,10,11). Important limitations can derive from the different experiences of radiologists in the interpretation of the multiparametric protocol: the inter-observational variability and the heterogeneity in the definition of positive and negative examination remain crucial and widely debated points.

Conventional MR images are qualitative, and their signal intensity is dependent on several complementary contrast mechanisms that are manipulated by the MR hardware and software. In the absence of a quantitative metric for absolute interpretation of pixel signal intensities, one that is independent of scanner hardware and sequences, it is difficult to perform comparisons of MR images across subjects or longitudinally in the same subject. Quantitative relaxometry isolates the contributions of individual MR contrast mechanisms (T1, T2, T2*) and provides maps, which are independent of the MR protocol and have a physical interpretation often expressed in absolute units. In addition to providing an unbiased metric for comparing MR scans, quantitative relaxometry uses the relationship between MR maps and physiology to provide a noninvasive surrogate for biopsy and histology (12).

There has been a need to develop methods imaging biomarkers such as T1 and T2 relaxation times maps and ADC maps from DWI, in order to develop quantitative and objective biomarkers that could combine with a radiological assessment, giving more objective parameters that could help the reader (13). Nevertheless, the MR signal intensity on standard sequence images does not significantly provide quantitative information. The same voxel with specific physical properties can have diverse intensities in different acquisitions conditional to many parameters, including the type and setup of the scanner (B0 and B1 heterogeneities, RF pulse profiles), and coils used, protocol-related issues such as vulnerability to parameter modification, reconstruction problems such as noise, echo spacing, calibration problems (phantoms-related) and others (14). Robust, fully quantitative multi-parametric acquisition, not scanner or configuration, has long been the goal of research in MRI, to increase objectivity in image analysis by providing absolute measurements and values, in a similar way to what has been done for computed tomography (CT) and Hounsfield Units (HU). However, the quantitative parameters that have been developed so far provide information on a single parameter at a time, their acquisition is time-consuming, and are often highly sensitive to scanner set-up. (14)

The development of quantitative MRI aims to increase objectivity in image investigation by providing absolute measurements. T2-mapping using MRI is a quantitative technique that can be used in prostate cancer evaluation, where a signal decay curve is derived from a series of T2w spin-echo sequences, and the T2 relaxation times of tissue can then be determined and encoded into a color parametric map (15). This technique might provide practical information based on the different sizes of the water compartments and different proportions of stromal and glandular tissue

between normal and malignant prostatic cancer, to complement anatomical and spatial information provided by standard T2w imaging (16).

This retrospective study aims to evaluate how T1 and T2 relaxation times, acquired on a 3 T scanner, are significant predictors of malignancy, correlating them with the PI-RADS v2.1 score.

Materials and methods

This is a retrospective, monocentric, observational study, which included 44 consecutive patients subjected to prostate MRI by regular clinical practice in the period from June 5, 2018, to April 30, 2019, in the PO secondary imaging center (blinded for peer-review). The IRB has approved this study; because of the retrospective nature, the informed consent patient was waived.

The inclusion criteria were a serum PSA value greater than four ng/ml and a positive outcome of digital rectal exploration.

We used the scanner of Canon Medical Systems Corporation (Ōtawara, Tochigi Prefecture, Japan) Vantage Titan 3T, model MRT-3010.

The sequences acquired for the study of the prostate are reported in Table 1 with the relative technical parameters. The T1 MP2RAGE (3D) and T2-multi-TE FSE2D sequences were highlighted, used in the dedicated workstation for image reconstruction with the Olea Sphere 3.0 software and the Olea Nova + plug-in (Olea Medical®, La Ciotat, France).

The T1 MP2RAGE (3D) sequence is characterized by a TR of 7.4 ms and a TE of 3.3 ms, a FOV of 250 x 250 mm with a 320 x 448 acquisition matrix, a flip angle of 8/9 degrees and a slice thickness of 3 mm. It has a scan time of 3:37 minutes.

The T2-multi-TE FSE2D sequence is characterized by a TR of 5012 ms and a TE of 20, 60, 100 and 140 ms, a FOV of 250 x 250 mm with a 384 x 448 acquisition matrix, a flip/refocus angle of 90/140 degrees and a slice thickness of 2.5 mm. It has a scan time of 10:52 minutes.

T2w, DWI, DCE, and Nova+ were acquired with the same position and slice thickness to allow direct comparison between sequences.

By visual analysis of the T2w, DWI, ADC, and DCE images from the PACS workstation, the lesions were identified by a radiologist with six years of experience, also considering the report already written by different radiologists who attributed the PI-RADS v2 score.

The same radiologist gave the assignment of a PI-RADS 2.1 assessment category for each lesion before

Table 1. Imaging parameters. The sequences used by the Olea Nova + software are highlighted.

Manufacturer, field strength	**Canon Medical Systems Corporation (ex Toshiba), 3 T**					
Model name	Vantage Titan 3T					
Receive coil type	Double 16-channels flex coil					
Sequence	*T1 MP2RAGE (3D)*	*T2-multi-TE FSE2D*	AX T2 Wide FOV	AX T2 Small FOV	DCE	AX DWI
TR (ms)	*7,4*	*5012*	8000	5684	5,2	3300
TE (ms)	*3,3*	*20, 60, 100, 140*	80	140	2,2	84
FOV (mm)	*250 × 250*	*250 × 250*	370 × 250	180 × 180	200 × 200	240 × 210
Acquisition matrix	*320 × 448*	*384 × 448*	256 × 384	256 × 256	128 × 128	128 × 112
Flip angle (degrees)	*8/9*	*90/140*	90/120	90/120	13	90/180
Slice thickness (mm)	*3*	*2,5*	5	3	3	5
Number of temporal acquisitions	*1*	*1*	2	3	1	5
Temporal resolution (s)	*3:37*	*10:52 (5:26/cover)*	4:08	5:13	7:44 (0:24)	11:34 (5:47)

analyzing the T1 and T2 maps, based on the scoring of T2w, DWI/ADC, and DCE sequences, according to zonal anatomy. (6)

The regions of interest (ROIs) were then traced in the corresponding areas of healthy and suspect neoplastic tissue in T1 and T2-mapping in the workstation with Olea Sphere 3.0, and average values were recorded. Lesions located in the PZ were distinguished from those located in the transition zone. ROIs were then traced in the ADC maps on healthy tissue and suspected neoplastic tissue. The average value of the ADC map in the ROI was recorded.

The pathological Gleason score was considered for 25 patients in the PZ and 18 patients in the TZ.

The serum PSA value was not considered since no data was available for all the patients.

Statistical analyzes were performed using SPSS software version 21.0 (IBM SPSS Statistics, Armonk, New York, USA) for Windows (Microsoft Corporation, Redmond, Washington, USA).

The normality of the continuous variables was tested with the Kolmogorov-Smirnov (KS) test.

The T1 and T2-relaxation times and ADC values were compared between healthy tissue and presumably pathological tissue with Wilcoxon signed-rank test.

The T1 and T2-relaxation times and ADC values were correlated with the values of PI-RADS v2 with Spearman's statistical test (Rho ρ).

A value of $p < 0.05$ was considered statistically significant.

Data were reported as mean ± sd.

Results

In the initial selection of 44 patients, 11 patients were excluded because the T1 MP2RAGE (3D) and T2-multi-TE FSE2D sequences were not acquired (n = 7) or because the T2 map was of poor quality (n = 4). This selection left a study population of 33 patients enrolled in a retrospective study consecutively from June 5, 2018, to April 30, 2019.

The subjects were men with an average age of 63 ± 8 years, in line with the national average, as stated in the guidelines of the American Urological Association (AUA) of 2018 (17).

Two patients had no suspicious prostate lesions (with PI-RADS 1 or 2, not reported), 19 patients had only one lesion, and 12 patients had two suspicious lesions (Figures 1 and 2).

Then 43 lesions were analyzed, 25 of them were in the PZ and 18 of them in the TZ.

15 lesions were classified as PIRADS 5 by the radiologist, 12 lesions as PIRADS 4, 13 lesions as PIRADS 3, and 3 lesions as PIRADS 2.

The Kolmogorov-Smirnov test showed that none of the variables is distributed in a normal way (Table 2).

The Wilcoxon signed-rank test showed statistically significant differences between T1-relaxation time of the tumor and healthy tissue of the PZ with a p-value of 0.043; statistically significant differences between T2-relaxation times of the tumor and healthy tissue of the PZ with a p-value of 0.043 (Table 3 and Table 4); statistically significant differences between ADC values of the tumor and healthy tissue of the PZ with a p-value of 0.043 (Table 3, Table 4); statistically significant differences between T1-relaxation time of the tumor and healthy tissue of the TZ with a p-value of= 0.018; a tendency to the difference between T2-relaxation times of the tumor and healthy tissue of the transition zone with a p-value of 0.062 (Table 3, Table 4); statistically significant differences between ADC values of the tumor and healthy tissue of the TZ with a p-value of 0.043 (Table 3, Table 4).

Figure 3 shows the graphical representation of the differences between T1 and T2 relaxation time and ADC values between healthy tissue and pathological suspect tissue, distinguishing the lesions of PZ and TZ.

The Spearman test (Tables 5 and 6) shows a tendency to a correlation between T2-relaxation time of the PZ and relative PI-RADS v2.1 scores with a p-value of 0.060; a tendency to a correlation between T1-relaxation time of the TZ and related PI-RADS v2 scores with a p-value of 0.053; a tendency to a correlation between ADC values of the PZ and relative PI-RADS v2.1 scores with a p-value of 0.072. The comparison between Gleason's score and PZ T2-relaxation times showed a tendency of correlation (p-value of 0.167). The remaining variables analyzed do not show significant correlations with statistically significant PI-RADS v2.1 score or correlation tendencies.

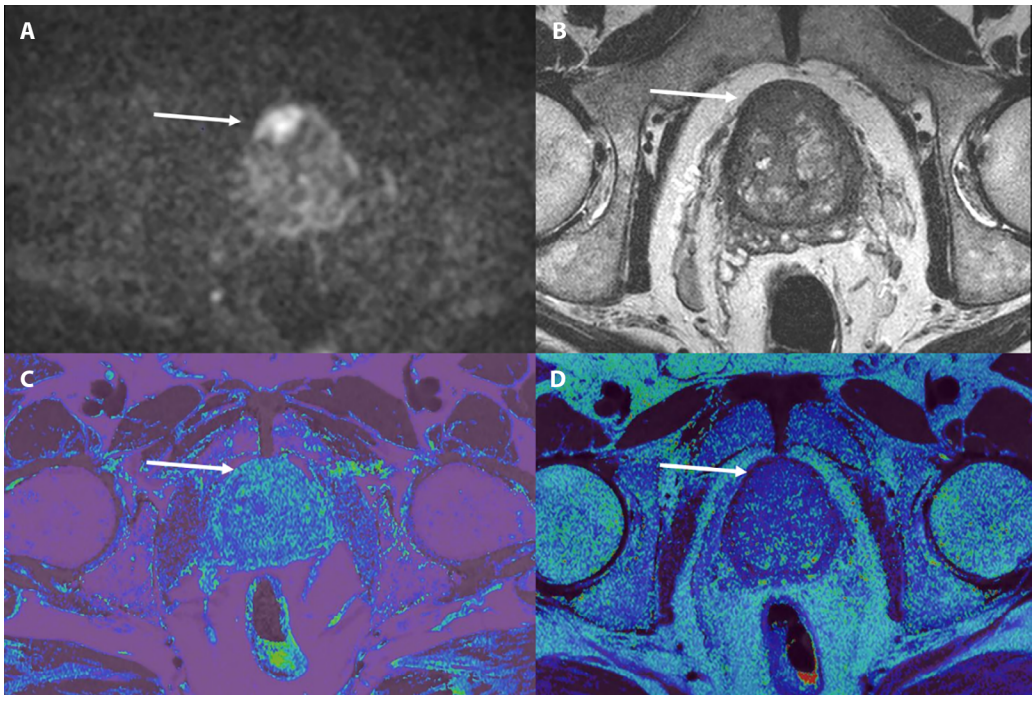

Figure 1. Example of a patient with a lesion in the right part of the central zone. A diffusion restriction (A, DWI, B 1600) and a hypointense T2 signal with blurred margins is seen (B), corresponding to a PIRADS vs 5. These lesions are not clearly visualized in the T1 (C), and T2 (D) maps. However, ROIs drawn in the lesion on the DWI and copied and pasted in the same position on the maps showed a different T1 of the lesion (1350 ms) vs the normal transition zone contralateral and a different T2 of the lesion (80 ms) vs the normal transition zone contralateral (128 ms).

Discussion

T2-mapping using MRI has already been used for the assessment of brain and cardiac tissue as well as changes in hyaline cartilage (18,19,20). This study shows that T1 and T2-mapping are also potentially useful in the assessment of prostate cancer. Given that T2w imaging is an essential MRI sequence for visualization of prostatic anatomy and evaluation of lesion morphology, T2-mapping could complement T2w in lesion analysis.

Our study shows that there is a significant difference between the T1 and T2-relaxation times of the pathological tissue and the healthy prostate, both for the TZ and the PZ. This reflects the intrinsic physical characteristics of the analyzed tissues, which are represented as relaxation times of transverse and longitudinal magnetization.

The relaxation times T1, T2, and T2* are physical parameters determined by intrinsic biophysical properties of tissue. The longitudinal relaxation time, T1, is a time constant describing the recovery of magnetization from a perturbed state to its equilibrium state The transverse relaxation time, T2, is a time constant describing the decay of magnetization that has been "excited" by a radiofrequency (RF) pulse (i.e., tipped into the transverse plane) that cannot be reversed by refocusing pulses (12).

T1 and T2-relaxation times of normal prostatic tissue change considerably according to the prostatic zone. T1 and T2-relaxation times of non-malignant tissue in the TZ are generally lower than in healthy tissue in the PZ. Given the increasing prevalence of benign prostatic hypertrophy (BPH) with age and the generally older age of the patients, this difference can probably be attributed to the presence of BPH in the TZ (21).

Overlap in the T2-relaxation times of malignant tissue and non-malignant tissue in the TZ can

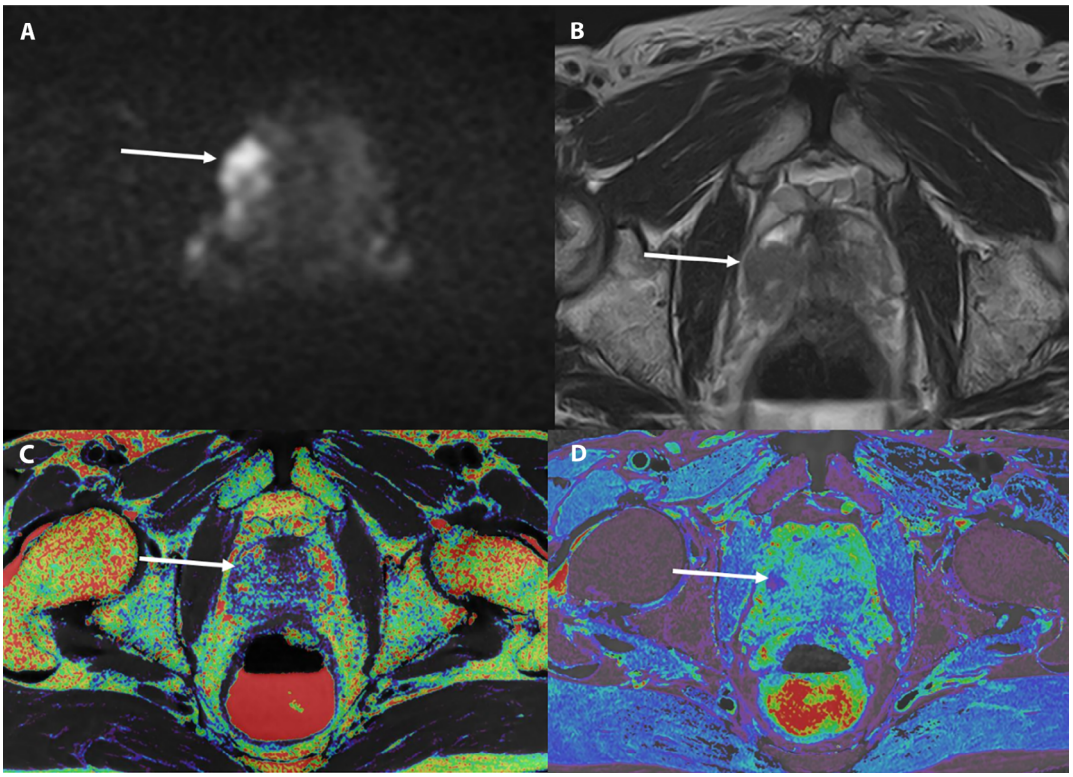

Figure 2. Example of a patient with a lesion in the peripheral zone. A diffusion restriction (A, DWI, B 1600) and a hypointense T2 signal is seen (B), corresponding to a PIRADS vs 5. This lesion is not clearly visualized in the T1 (C) but is clearly seen T2 (D) maps. However, ROIs drawn in the lesion on the DWI and copied and pasted in the same position on the maps showed a different T1 of the lesion (1450 ms) vs the normal peripheral zone contralateral (2000 ms) and a different T2 of the lesion (60 ms) vs the normal peripheral zone contralateral (255 ms).

Table 2. Lilliefors significance correction.

			Statistic	df
Peripheral zone	lesion	Average T1	0,265	3
		Average T2	0,324	3
		ADC values	0,203	3
	normal	Average T1	0,367	3
		Average T2	0,252	3
		ADC values	0,212	3
Transitional zone	lesion	Average T1	0,219	3
		Average T2	0,196	3
		ADC values	0,342	3
	normal	Average T1	0,368	3
		Average T2	0,385	3
		ADC values	0,271	3

probably be attributed to the presence of BPH. BPH demonstrates a heterogeneous range of MRI features: nodules can range in intensity depending on the composition of glandular, fibromuscular, and stromal elements (22), and it can be challenging to distinguish BPH and prostate cancer (23).

The distinction between healthy and tumoral prostatic tissue appears more straightforward in the PZ, where T1 and T2-relaxation times of malignant tissue have been shown to be lower than healthy tissue in the PZ (24).

Regarding the ADC maps, the values we found for both healthy and pathological tissue are in line with values already found by Shaish, H. et al. (25). Also with regard to the average values of T1 and T2 relaxation time our values for both healthy and pathological

Table 3. a. On the left, the blue table, Wilcoxon Signed Ranks Test; b. On the right, the rose table, based on negative ranks.

Test Statistics[a]						
	Peripheral zone			Transitional zone		
	T1-relaxation time normal and pathological	T2-relaxation time normal and pathological	ADC values normal and pathological	T1-relaxation time normal and pathological	T2-relaxation time normal and pathological	ADC values normal and pathological
Z	-2,023[b]	-2,023[b]	-2,023[b]	-2,366[b]	-1,859[b]	-2,023[b]
Asymp. Sig. (2-tailed)	0,043	0,043	0,043	0,018	0,063	0,043

Table 4. Statistical analysis based on PI-RADS: differences between T1-relaxation time of the tumor and healthy tissue of the TZ; difference between T2-relaxation times of the tumor and healthy tissue of the transition zone; differences between ADC values of the tumor and healthy tissue of the TZ. All of there were statistically significant differences.

	PI-RADS v2.1 score	Average T1-relaxation time (ms)	Average T2-relaxation time (ms)	Average ADC values (mm^2/s)
Peripheral zone	3	1645 ± 202	104 ± 3	868 ± 38
	4	1536 ± 220	89 ± 9	705 ± 434
	5	1404 ± 401	74 ± 34	670 ± 148
Transitional zone	3	1746 ± 38	95 ± 21	693 ± 176
	4	1575 ± 146	90 ± 7	718 ± 122
	5	1516 ± 228	86 ± 8	610 ± 168

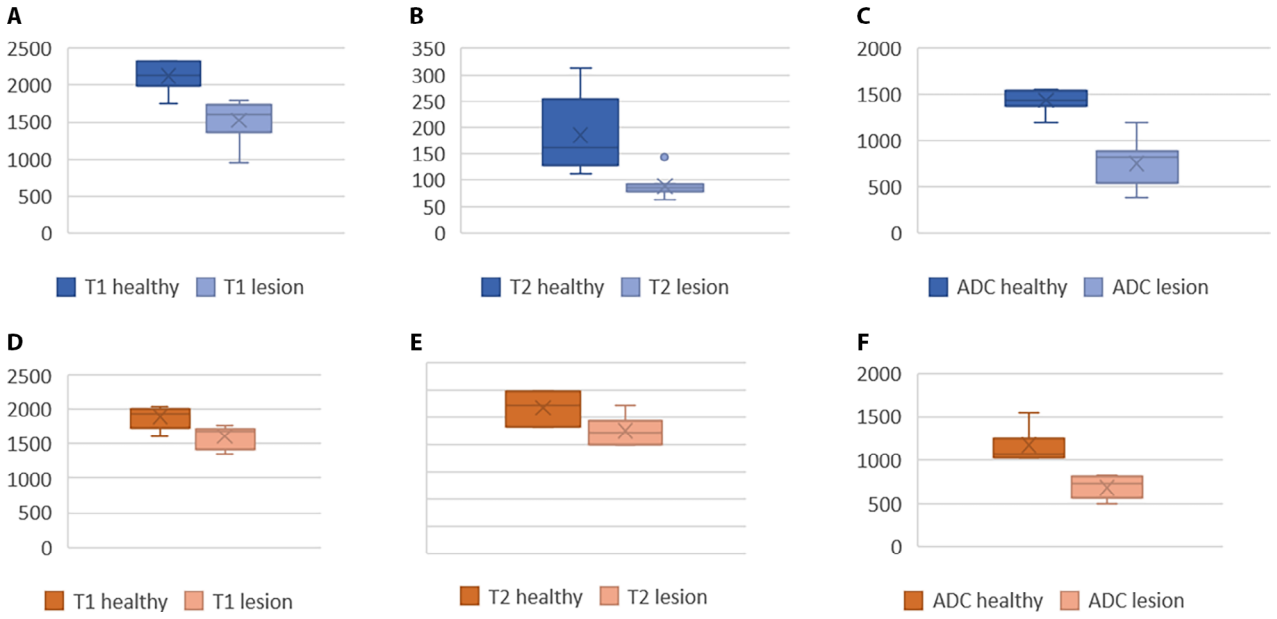

Figure 3. A Differences between T1 values of healthy and neoplastic tissue in the peripheral zone; B Differences between T2 values of healthy and neoplastic tissue in the peripheral zone; C Differences between ADC values of healthy and neoplastic tissue in the peripheral zone; D Differences between T1 values of healthy and neoplastic tissue in the transition zone; E Differences between T2 values of healthy and neoplastic tissue in the transition zone; F Differences between ADC values of healthy and neoplastic tissue in the transition zone.

Table 5. The Spearman test used to identify a correlation between T2-relaxation time of the PZ and relative PI-RADS v2.1 scores, a correlation between T1-relaxation time of the TZ and related PI-RADS v2 scores and a correlation between ADC values of the PZ and relative PI-RADS v2.1 scores.

			Average T1-relaxation time	Average T2-relaxation time	Average ADC values
Spearman's rho	**PI-RADS v2.1 (Peripheral zone)**	**Correlation Coefficient**	-0,369	-0,556	-0,527
		Sig. (1-tailed)	0,164	0,060	0,072
		N	25	25	25
			Average T1-relaxation time	**Average T2-relaxation time**	**Average ADC value**
Spearman's rho	**PI-RADS v2.1 (Transition zone)**	**Correlation Coefficient**	-0,661	-0,191	-0,283
		Sig. (1-tailed)	0,053	0,341	0,269
		N	18	18	18

Table 6. The Spearman test used to identify a correlation between Gleason's score and PZ T2-relaxation times.

			Average T1-relaxation time	Average T2-relaxation time	Average ADC values
Spearman's rho	**Gleason (Peripheral zone)**	**Correlation Coefficient**	-0,563	-0,167	-0,612
		Sig. (1-tailed)	0,321	0,231	0,032
		N	25	25	25
			Average T1-relaxation time	**Average T2-relaxation time**	**Average ADC value**
Spearman's rho	**Gleason (Transition zone)**	**Correlation Coefficient**	-0,651	-0,456	-0,541
		Sig. (1-tailed)	0,034	0,035	0,049
		N	18	18	18

tissue are in line with values already found by Fennessy, F. M. et al. (26) and by Yamauchi, F. I. et al. (27).

One of the biggest issues to be solved of quantitative MRI is to find threshold values that reliably differentiate malignant and benign prostate tissue and how this can be translated to clinical routine.

A limitation of this study is the reduced number of patients as it does not yet allow us to establish a cut-off value between pathological and benign tissue. However, looking at the T2 map alone, all pathological tissue in our study has a T2 relaxation time shorter than 100 ms, and all non-pathological tissues have a T2 time longer than 100 ms.

Additional limitations are the subjectivity in the attribution of the PI-RADS score, which has been widely criticized by the existing literature (9,10).

Our study agrees with the systematic review of the literature by Lee Chau Hung (28) which takes into consideration 17 studies in the year 2018, that measured T2 relaxation times of malignant and healthy prostatic tissue. This systematic review on T2-mapping shows that there is a range of T2-relaxation times in healthy prostatic tissue. This has been linked to the fact that healthy prostatic tissue consists of glands which contain fluid (with long T2-relaxation times) enclosed by epithelium and stroma (with short T2-relaxation times), resultant in a pattern of T2 relaxation which has two peaks (29). The high prevalence of BPH in the elderly, which can have similar imaging features as prostate cancer, also makes finding a reliable threshold more problematic. The standardization of the quantitative measurements using different MRI systems or software and standardization of acquisition parameters are also important considerations when translating quantitative MRI in clinical practice (30).

Quantitative MRI techniques could theoretically lead to the disappearing of DCE-MRI, which is of interest, given the rising concern regarding gadolinium harmfulness and its reduced emphasis in the latest PI-RADS versions (31,32,33).

T2-mapping is useful in evaluation of cancers in the PZ but is unable to distinguish between TZ cancers and BPH reliably. Valuation of lesion morphology and margins on T2W MRI is still essential when evaluating for TZ cancers. Further analysis is recommended to study if T2-mapping increases diagnostic performance when utilized in conjunction with subjective evaluation of prostate cancer.

The differences in T1 and T2-relaxation time in healthy and tumoral tissues could help both the radiologist in the detection of tumors, but also the development of artificial intelligence algorithms (34,35) that could exploit even more deeply these intrinsic properties.

This data should be investigated with studies with a higher number of patients.

Synthetic MRI is a translation of absolute maps into conventional contrast images, so a single quantitation scan can provide both absolute maps and regular contrast images for the radiologist's analysis (14). A multicenter prospective multi-reader case-control study of the global image quality of synthetic MRI versus conventional MRI in a general population showed that synthetic MRI is not inferior to conventional, with a comparable diagnostic utility for recognition of a series of brain pathologies. Since synthetic reconstructions are based mainly on the quality of a single acquisition, attention must be paid to minimize motion and other artifacts (36).

Post-processing software for Synthetic MRI is available in the commercial product SyMRI from SyntheticMR AB, which is included as an option called MAGiC on the MR console for GE's SIGNA Pioneer 3T MRI scanner. Since 2017, synthetic MRI is also available on Siemens (Erlangen, Germany) machines. Olea Medical (Canon Group) offers a similar product named Olea Nova+. Olea utilizes a method for automatic computing of standard MRI weighted images from a protocol that acquires images to derive T1 and T2 maps. Users are able to create images with any contrast-weighting in T1, T2 or maps by varying TE, TR or TI.

The future perspective is to search, through the T1 and T2 mappings, for the cut-off values that can allow identifying with absolute certainty the pathological tissues. This is essential for reproducibility with the various commercially available scanners and, therefore, the clinical validation of synthetic magnetic resonance. T1 and T2 maps can be used to extract radiomics features which would reflect intrinsic physical properties of the tissues (relaxation times) instead of pixel intensities (37,38,39). These maps could also be used by an artificial intelligence algorithm that would exploit the subtle differences, probably allowing to recognize early cancers (40,41,42).

Conclusion

In conclusion, T1-and T2-mapping can represent a valid method to support the detection of tumors in prostatic resonance and seem to correlate with the severity of the lesions themselves, as emerges from the correlative analyses. Although not statistically significant, there would appear to be a tendency for correlation between lower T2-relaxation times and higher PI-RADS v2.1 score, particularly in the transition zone. Further studies are recommended to determine

if T1 and T2-mapping increase diagnostic performance when utilized in conjunction with mpMRI for the detection of prostate cancer and the assignment of PI-RADS v2.1 score.

Abbreviations: ADC: Apparent Diffusion Coefficient; DCE: dynamic contrast-enhanced; DWI: diffusion-weighted imaging; mpMRI: multiparametric Magnetic Resonance Imaging; PI-RADS: Prostate Imaging Reporting and Data System; ROI: Region of interest; T2w T2: weighted; TE time echo; TI: inversion time; TR: repetition time.

Conflict of Interest: Each author declares that he or she has no commercial associations (e.g. consultancies, stock ownership, equity interest, patent/licensing arrangement etc.) that might pose a conflict of interest in connection with the submitted article.

Authors Contribution: All authors contributed to the study conception and design. Material collection was performed by all authors. All authors participated in the writing of the paper. All authors read and approved the final manuscript.

References

1. Turkbey B, Rosenkrantz AB, Haider MA, et al. Prostate imaging reporting and data system version 2.1: 2019 update of prostate imaging reporting and data system version 2. Eur Urol. 2019 Sep;76(3):340-351. doi:10.1016/j.eururo.2019.02.033
2. Hegde JV, Mulkern RV, Panych LP, et al. Multiparametric MRI of prostate cancer: an update on state-of-the-art techniques and their performance in detecting and localizing prostate cancer. J Magn Reson Imaging. 2013 May;37(5):1035–54. doi:10.1002/jmri.23860
3. Carpagnano FA, Eusebi L, Tupputi U, et al. Multiparametric MRI: Local Staging of Prostate Cancer. Curr Radiol Rep. 2020 Dec;8(12):27. doi: 10.1007/s40134-020-00374-y
4. Barentsz JO, Richenberg J, Clements R, et al. ESUR prostate MR guidelines 2012. Eur Radiol. 2012 Apr;22(4):746–57. doi:10.1007/s00330-011-2377-y
5. Payne GS, Leach MO. Applications of magnetic resonance spectroscopy in radiotherapy treatment planning. Br J Radiol. 2006 Sep;79(special_issue_1):S16–26. doi:10.1259/bjr/84072695
6. Weinreb JC, Barentsz JO, Choyke PL, et al. PI-RADS Prostate Imaging – Reporting and Data System: 2015, Version 2. Eur Urol. 2016 Jan;69(1):16–40. doi:10.1016/j.eururo.2015.08.052
7. Mottet N, Bellmunt J, Bolla M, et al. EAU-ESTRO-SIOG Guidelines on Prostate Cancer. Part 1: Screening, Diagnosis, and Local Treatment with Curative Intent. Eur Urol. 2017 Apr;71(4):618–29. doi:10.1016/j.eururo.2016.08.003
8. Cornford P, Bellmunt J, Bolla M, et al. EAU-ESTRO-SIOG Guidelines on Prostate Cancer. Part II: Treatment of Relapsing, Metastatic, and Castration-Resistant Prostate Cancer. Eur Urol. 2017 Apr;71(4):630–42. doi:10.1016/j.eururo.2016.08.002
9. Garcia-Reyes K, Passoni NM, Palmeri ML, et al. Detection of prostate cancer with multiparametric MRI (mpMRI): effect of dedicated reader education on accuracy and confidence of index and anterior cancer diagnosis. Abdom Imaging. 2015 Jan;40(1):134–42. doi:10.1007/s00261-014-0197-7
10. Greer MD, Brown AM, Shih JH, et al. Accuracy and agreement of PIRADSv2 for prostate cancer mpMRI: A multireader study. J Magn Reson Imaging. 2017 Feb;45(2):579–85. doi:10.1002/jmri.25372
11. Ventrella E, Eusebi L, Carpagnano FA, Bartelli F, Cormio L, Guglielmi G. Multiparametric MRI of Prostate Cancer: Recent Advances. Curr Radiol Rep. 2020 Oct;8(10):19. https://doi.org/10.1007/s40134-020-00363-1
12. Margaret Cheng H-L, Stikov N, Ghugre NR, Wright GA. Practical medical applications of quantitative MR relaxometry. J Magn Reson Imaging. 2012 Oct;36(4):805–24. doi:10.1002/jmri.23718
13. (ESR) ES of R. ESR statement on the stepwise development of imaging biomarkers. Insights Imaging. 2013 Apr;4(2):147–52. doi:10.1007/s13244-013-0220-5
14. (ESR) ES of R. Magnetic Resonance Fingerprinting - a promising new approach to obtain standardized imaging biomarkers from MRI. Insights Imaging. 2015 Apr;6(2):163–5. doi:10.1007/s13244-015-0403-3
15. Nöth U, Shrestha M, Schüre J-R, Deichmann R. Quantitative in vivo T2 mapping using fast spin echo techniques – A linear correction procedure. NeuroImage. 2017 Aug;157:476–85. doi:10.1016/j.neuroimage.2017.06.017
16. Nguyen K, Sarkar A, Jain AK. Prostate Cancer Grading: Use of Graph Cut and Spatial Arrangement of Nuclei. IEEE Trans Med Imaging. 2014 Dec;33(12):2254–70. doi:10.1109/TMI.2014.2336883
17. Carter HB, Albertsen PC, Barry MJ, et al. Early Detection of Prostate Cancer: AUA Guideline. J Urol. 2013 Aug;190(2):419–26. doi:10.1016/j.juro.2013.04.119
18. Kim PK, Hong YJ, Im DJ, et al. Myocardial T1 and T2 Mapping: Techniques and Clinical Applications. Korean J Radiol. 2017;18(1):113–31. doi:10.3348/kjr.2017.18.1.113
19. Knight MJ, McCann B, Tsivos D, Dillon S, Coulthard E, Kauppinen RA. Quantitative T2 mapping of white matter: applications for ageing and cognitive decline. Phys Med Biol. 2016 Aug;61(15):5587–605. doi:10.1088/0031-9155/61/15/5587
20. Mamisch TC, Trattnig S, Quirbach S, Marlovits S, White LM, Welsch GH. Quantitative T2 Mapping of Knee Cartilage: Differentiation of Healthy Control Cartilage and Cartilage Repair Tissue in the Knee with Unloading—Initial Results. Radiology. 2010 Mar;254(3):818–26. doi:10.1148/radiol.09090335

21. Lim K Bin. Epidemiology of clinical benign prostatic hyperplasia. Asian J Urol. 2017 Jul;4(3):148–51. doi:10.1016/j.ajur.2017.06.004
22. Guneyli S, Ward E, Thomas S, et al. Magnetic resonance imaging of benign prostatic hyperplasia. Diagn Interv Radiol. 2016 May;22(3):215–9. doi:10.5152/dir.2015.15361
23. Chesnais AL, Niaf E, Bratan F, et al. Differentiation of transitional zone prostate cancer from benign hyperplasia nodules: Evaluation of discriminant criteria at multiparametric MRI. Clin Radiol. 2013 Jun;68(6):e323–30. doi:10.1016/j.crad.2013.01.018
24. Panda A, Obmann VC, Lo W-C, et al. MR Fingerprinting and ADC Mapping for Characterization of Lesions in the Transition Zone of the Prostate Gland. Radiology. 2019 Sep;292(3):685–94. doi:10.1148/radiol.2019181705
25. Shaish H, Kang SK, Rosenkrantz AB. The utility of quantitative ADC values for differentiating high-risk from low-risk prostate cancer: a systematic review and meta-analysis. Abdom Radiol. 2017 Jan;42(1):260–70. doi:10.1007/s00261-016-0848-y
26. Fennessy FM, Fedorov A, Gupta SN, Schmidt EJ, Tempany CM, Mulkern R V. Practical considerations in T1 mapping of prostate for dynamic contrast enhancement pharmacokinetic analyses. Magn Reson Imaging. 2012 Nov;30(9):1224–33. doi:10.1016/j.mri.2012.06.011
27. Yamauchi FI, Penzkofer T, Fedorov A, et al. Prostate cancer discrimination in the peripheral zone with a reduced field-of-view T(2)-mapping MRI sequence. Magn Reson Imaging. 2015 Jun;33(5):525–30. doi:10.1016/j.mri.2015.02.006
28. Lee CH. Quantitative T2-mapping using MRI for detection of prostate malignancy: a systematic review of the literature. Acta Radiol. 2019;60(9):1181-1189. doi:10.1177/0284185118820058
29. Bourne RM, Kurniawan N, Cowin G, et al. Biexponential diffusion decay in formalin-fixed prostate tissue: Preliminary findings. Magn Reson Med. 2012 Sep;68(3):954–9. oi:10.1002/mrm.23291
30. Hoang Dinh A, Souchon R, Melodelima C, et al. Characterization of prostate cancer using T2 mapping at 3T: A multi-scanner study. Diagn Interv Imaging. 2015 Apr;96(4):365–72. doi:10.1016/j.diii.2014.11.016
31. Prince MR, Lee HG, Lee C-H, et al. Safety of gadobutrol in over 23,000 patients: the GARDIAN study, a global multicentre, prospective, non-interventional study. Eur Radiol. 2017 Jan;27(1):286–95. doi:10.1007/s00330-016-4268-8
32. Gulani V, Calamante F, Shellock FG, Kanal E, Reeder SB. Gadolinium deposition in the brain: summary of evidence and recommendations. Lancet Neurol. 2017 Jul;16(7):564–70. doi:10.1016/S1474-4422(17)30158-8
33. Purysko AS, Rosenkrantz AB, Barentsz JO, Weinreb JC, Macura KJ. PI-RADS Version 2: A Pictorial Update. RadioGraphics. 2016 Sep;36(5):1354–72. doi:10.1148/rg.2016150234
34. Hosny A, Parmar C, Quackenbush J, Schwartz LH, Aerts HJWL. Artificial intelligence in radiology. Nat Rev Cancer. 2018 Aug;18(8):500–10. doi:10.1038/s41568-018-0016-5
35. What the radiologist should know about artificial intelligence - an ESR white paper. Insights Imaging. 2019;10(1):44. Published 2019 Apr 4. doi:10.1186/s13244-019-0738-2ec;10(1):44.
36. Tanenbaum LN, Tsiouris AJ, Johnson AN, et al. Synthetic MRI for Clinical Neuroimaging: Results of the Magnetic Resonance Image Compilation (MAGiC) Prospective, Multicenter, Multireader Trial. AJNR Am J Neuroradiol. 2017 Jun;38(6):1103–10. doi:10.3174/ajnr.A5227
37. Cameron A, Khalvati F, Haider MA, Wong A. MAPS: A Quantitative Radiomics Approach for Prostate Cancer Detection. IEEE Trans Biomed Eng. 2016 Jun;63(6):1145–56. doi:10.1109/TBME.2015.2485779
38. Stoyanova R, Takhar M, Tschudi Y, et al. Prostate cancer radiomics and the promise of radiogenomics. Transl Cancer Res. 2016 Aug;5(4):432–47. doi:10.21037/tcr.2016.06.20
39. Sun Y, Reynolds HM, Parameswaran B, et al. Multiparametric MRI and radiomics in prostate cancer: a review. Australas Phys Eng Sci Med. 2019 Mar;42(1):3–25. doi:10.1007/s13246-019-00730-z
40. Goldenberg SL, Nir G, Salcudean SE. A new era: artificial intelligence and machine learning in prostate cancer. Nat Rev Urol. 2019;16(7):391-403. doi:10.1038/s41585-019-0193-3
41. Harmon SA, Tuncer S, Sanford T, Choyke PL, Turkbey B. Artificial intelligence at the intersection of pathology and radiology in prostate cancer. Diagn Interv Radiol. 2019 May;25(3):183–8. doi:10.5152/dir.2019.19125
42. Wong NC, Shayegan B. Patient centered care for prostate cancer—how can artificial intelligence and machine learning help make the right decision for the right patient? Ann Transl Med. 2019 Mar;7(S1):S1–S1. doi:10.21037/atm.2019.01.13

Correspondence:
Received: 22 December 2022
Accepted: 4 September 2023
Giuseppe Guglielmi, Prof., MD
Department of Clinical and Experimental Medicine, Foggia University School of Medicine, Viale
L. Pinto 1, 71121, Foggia, Italy;
Radiology Unit, "Dimiccoli" Hospital, Viale Ippocrate, 15, 70051 Barletta, Italy;
Radiology Unit, IRCCS "Casa Sollievo della Sofferenza" Hospital, Viale Cappuccini 2,
71013 San Giovanni Rotondo, FG, Italy
E-mail: giuseppe.guglielmi@unifg.it